Letter

Unconventional vortex lattice and topological defects in rigidly rotating multicomponent superfluids

Roy Rabaglia,[1] Ryan L. Barnett,[2] and Ari M. Turner[1]
[1]*Department of Physics, Technion, Haifa 32000, Israel*
[2]*Department of Mathematics, Imperial College London, London SW7 2AZ, United Kingdom*

(Received 29 May 2024; revised 2 July 2025; accepted 14 October 2025; published 17 November 2025)

By examining rotating ferromagnetic spinor condensates through the perspective of large spin, we identify an atypical type of topological point defects in the magnetization texture. These defects are not predicted by conventional homotopy analysis but rather by the Riemann-Hurwitz formula. The magnetization texture in the system is described by an equal-area mapping from the plane to the sphere of magnetization, forming a lattice of uniformly charged skyrmions. This lattice contains doublyquantized (winding number = 2) point defects arranged on the sphere in a tetrahedral configuration. The fluid is found to be rotating rigidly, except at the point defects, where the vorticity vanishes. This vorticity structure describes an unconventional "unvortex" lattice, which contrasts with the well-known vortex lattice in scalar rotating superfluids, where vorticity is concentrated exclusively within defect points. Numerical results are presented, confirming these predictions and demonstrating their persistence in smaller-spin condensates.

DOI: 10.1103/jcpc-c3vb

One fundamental characteristic of ordinary (scalar) superfluids is their irrotational flow. In contrast, spinor Bose–Einstein condensates exhibit an intrinsic coupling between the superfluid velocity field $\mathbf{v}(\mathbf{r})$ and the magnetization unit vector field $\hat{\mathbf{n}}(\mathbf{r})$. This coupling is governed by the well-known *Mermin-Ho relation* [1],

$$(\boldsymbol{\nabla}\times\mathbf{v})_k = \frac{\hbar}{2m}F\varepsilon_{ijk}\hat{\mathbf{n}}\cdot(\partial_i\hat{\mathbf{n}}\times\partial_j\hat{\mathbf{n}}), \tag{1}$$

where m and F are the mass and spin of the condensed particles, respectively. For a planar ($d=2$) condensate, this relation has an intriguing geometrical interpretation: the right-hand side is proportional to the Jacobian $J(\mathbf{r})$ of the transformation $\hat{\mathbf{n}}(\mathbf{r}):\mathbb{R}^2\to\mathbb{S}^2$, mapping the physical space to the sphere of spin states.

A rich variety of magnetization textures and flow fields are known to occur in spinor condensates [2–20]. One such phenomenon, facilitated by the Mermin-Ho relation, is the elimination of the need for vortices with diverging velocity [21–23]. In its ground state, a nonrotating ferromagnetic condensate features uniform magnetization. Upon rotation, maintaining uniform magnetization would lead to an irrotational flow around a lattice of quantized vortices, as in ordinary superfluids. However, the Mermin-Ho relation enables the system to reduce its energy by adopting nonuniform magnetization, leading to a nontrivial flow field [3,4,24–26]. While a uniform circulation matching rigid rotation might seem energetically favorable, we show that a unique class of defects induces large variations in circulation.

This discussion is based on an original analytical approach to understand properties of spinor condensates, by inspecting the system from the viewpoint of large spin ($F\gg 1$). Experimental realizations of spinor condensates have so far reached total spin values up to $F=8$ [27–40]. This range already allows exploration of the large-F behavior discussed here. We show that the large spin viewpoint is capable not only of capturing the properties of the larger spin condensates, but can even provide a framework for understanding smaller-spin condensates, such as spin 1. Expansions around $F=\infty$ can be combined with results of expansions around $F=0$, which we will present in future work [41], to provide a fairly accurate description of condensates of any spin value.

We use this system as a framework to introduce a unique kind of topological defects, which constitute the central focus of this paper. These defects, which emerge in the magnetic texture, are naturally understood from the large-F viewpoint, yet they persist in systems regardless of the spin value. Their impact on the system is profound, influencing various properties beyond the magnetic texture itself, such as the aforementioned regions of depleted vorticity, which form around the magnetic defects and disrupt an otherwise rigid flow. The resulting vorticity structure (see Fig. 1), stands as an antithesis to the traditional vortex lattice in superfluids, where all the vorticity is concentrated within the defects.

These defects arise from a mechanism distinct from that of standard topological defects and do not fit within the standard classification schemes such as homotopy theory; they result from the Riemann-Hurwitz formula, a relationship that constrains mappings between topologically inequivalent spaces. Similar to the planar case, these defects also persist in the ground state of three-dimensional condensates, forming a lattice of line defects. These can be studied for behaviors such as bending or knotting, akin to defects in conventional superfluids [42–44]. We believe that this special type of defects might also be relevant to physical systems far beyond spinor condensates, such as quantum Hall systems, where skyrmions emerge and their number is fixed by the deviation from special filling fractions [45], or blue phase of liquid crystals in which the energy is minimized by having a texture of the nematic that varies in a noncoplanar way, where results analogous to the Mermin-Ho relation can be used [46,47].

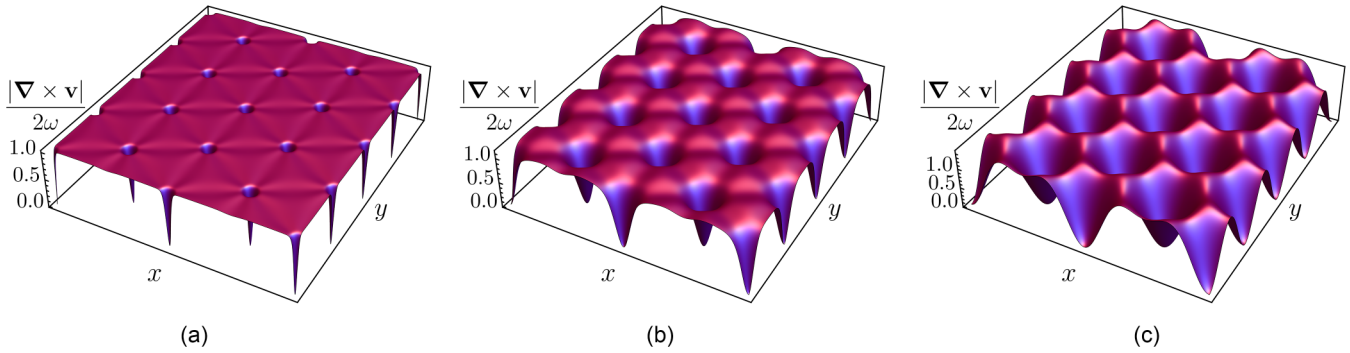

FIG. 1. The "unvortex" lattice, obtained numerically for (a) $F = 100$, (b) $F = 8$, (c) $F = 1$. A triangular lattice of low vorticity cores forms around each point defect, which are predicted by the Riemann-Hurwitz formula. For large F, the condensate rotates rigidly between the cores.

Spinor condensates can exhibit various phases determined by the interatomic interaction parameters [2,48,49]. Our focus is on the ferromagnetic phase, which can occur for any spin F within a certain range of the spin-dependent interaction parameters. Assuming a constant density profile [50], the condensate in this phase can be described solely by the two fields $\mathbf{v}(\mathbf{r})$ and $\hat{\mathbf{n}}(\mathbf{r})$. An alternative description involves angles: the superfluid phase $\theta(\mathbf{r})$ and the magnetic polar and azimuthal angles $\phi(\mathbf{r})$ and $\chi(\mathbf{r})$. Using these angles, the magnetization texture is $\hat{\mathbf{n}} = (\sin\phi\cos\chi, \sin\phi\sin\chi, \cos\phi)$, and the velocity field in the nonrotating frame of reference is [51]

$$\mathbf{v}(\mathbf{r}) = \frac{\hbar}{m}[\nabla\theta - F\cos\phi\nabla\chi]. \tag{2}$$

Taking the curl yields the Mermin-Ho relation, Eq. (1):

$$\nabla \times \mathbf{v} = \frac{\hbar}{m} F J(\mathbf{r})\hat{\mathbf{z}}. \tag{3}$$

In terms of ϕ and χ, the Jacobian can be written as $J(\mathbf{r}) = \sin\phi(\nabla\phi \times \nabla\chi)\cdot\hat{\mathbf{z}}$. When rotated with an angular velocity of $\boldsymbol{\omega} = \omega\hat{\mathbf{z}}$, the energy functional of the system is [50–52]

$$E = \frac{\hbar^2\rho}{2m}\int \mathrm{d}^2 r\left[\frac{m^2}{\hbar^2}(\mathbf{v} - \boldsymbol{\omega}\times\mathbf{r})^2 + \frac{1}{2}F\left(\nabla\hat{\mathbf{n}}\right)^2\right]. \tag{4}$$

We want to identify the important contributions in the large-F limit. Although a cursory examination of the energy functional may seem to suggest a dominance of the second (magnetic) term, this overlooks the F dependence of the velocity field, as indicated in Eq. (2). This expression for the velocity field contains a term proportional to F, hence the first (kinetic) term in the energy contains terms proportional to F^2. This surprisingly indicates its dominance over the magnetic term, which is proportional only to F. To show this rigorously, we propose employing a rescaling technique.

We rescale the lengths using $\tilde{\mathbf{r}} = F^{-1/2}\mathbf{r}$ to eliminate the dependence of the magnetic term on F, and the phase using $\tilde{\theta} = F^{-1}\theta$ to simplify the resulting expression. After these rescalings, the velocity field becomes

$$\tilde{\mathbf{v}} = \frac{1}{\sqrt{F}}\mathbf{v} = \frac{\hbar}{m}[\tilde{\nabla}\tilde{\theta} - \cos\phi\tilde{\nabla}\chi] \tag{5}$$

and contains no explicit dependence on F. As velocity measures the change in position over time, it was also rescaled to account for the rescaling of lengths. The energy, which is similarly rescaled by $\tilde{E} = F^{-1}E$, becomes

$$\tilde{E} = \frac{\hbar^2\rho}{2m}\int \mathrm{d}^2\tilde{r}\left[\frac{m^2}{\hbar^2}F(\tilde{\mathbf{v}} - \boldsymbol{\omega}\times\tilde{\mathbf{r}})^2 + \frac{1}{2}(\tilde{\nabla}\hat{\mathbf{n}})^2\right]. \tag{6}$$

As we will use only the rescaled quantities, we omit the tilde symbol in subsequent equations. Unlike the original energy functional (4), the rescaled energy functional exhibits a remarkably simple dependence on F. After rescaling, it is clear that the dominant term in the large-F limit is the kinetic one. Deviations from a state minimizing this term result in a high energetic cost, implying that the condensate rotates rigidly, such that $\mathbf{v} = \boldsymbol{\omega}\times\mathbf{r}$. A previous proposal to realize rigidly rotating superfluids involves the use of spin-orbit coupling [53]. Our study predicts a natural occurrence of this phenomenon in large-F spinor condensates.

The vorticity for rigid rotation is a constant, $2\boldsymbol{\omega}$, implying a constant Jacobian $J(\mathbf{r}) = 2m\omega/\hbar F$ according to the Mermin-Ho relation (3). Therefore, the mapping $\hat{\mathbf{n}}(\mathbf{r})$ must be *area-preserving* (up to a constant scaling factor). We will assume $\omega > 0$, and therefore $J(\mathbf{r})$ is positive.

Such a mapping can also be considered as describing a system with uniform skyrmionic charge density, where the skyrmionic charge $Q = 1/4\pi\int J(\mathbf{r})\mathrm{d}^2 r$ is the number of times the sphere is covered by the mapping in each unit cell [24,54,55]. This provides us with an equation for the area A of the unit cell in terms of Q:

$$A = \frac{2\pi\hbar}{m\omega}FQ. \tag{7}$$

Any periodic, area-preserving mapping from the plane to the sphere, or more generally, any mapping with a single-sign Jacobian, must have defects. These defects can appear in various forms, such as lines or points. Our focus is on point defects, as other types of singularities incur a large energetic cost. The defects of the type we consider will occur in a mapping from a two-dimensional system to a two-dimensional order parameter space (but can be generalized to higher dimensions). We assume that a mapping $\hat{\mathbf{n}} : P \to S$ with a positive Jacobian is favored. For each point like this, a sufficiently small region around it will be mapped in a one-to-one way to a region of the order parameter space. Conversely, a defect is a point p with the property that a small disk around p, with p removed from it, is mapped in a k-to-one way to the order parameter space, for $k \geqslant 2$. As a result, the

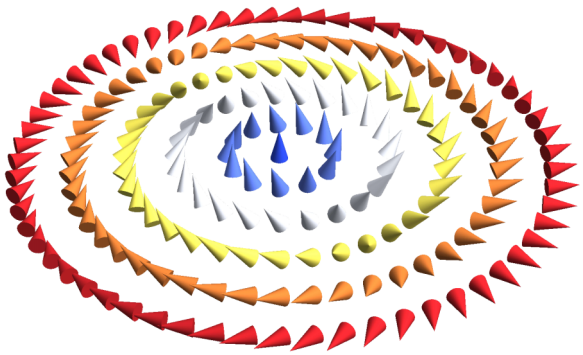

FIG. 2. An illustration of the magnetic texture (8) for $k = 2$. Each magnetization vector is the image of two different points, except for the magnetization of the defect itself at the origin.

Jacobian must vanish in these specific points, as the mapping is not invertible in their neighborhood. These defects have the same topological structure as branching points of analytic mappings.

An example of such a defect is at the origin of the following texture, using the polar coordinates (r, α):

$$\hat{\mathbf{n}}(\mathbf{r}) = (\sin\phi(r)\cos(k\alpha), \sin\phi(r)\sin(k\alpha), \cos\phi(r)), \quad (8)$$

where $\phi(r) \to 0$ as $r \to 0$. This field corresponds to the azimuthal angle $\chi = k\alpha$, having a winding number of k for this angle. As can be seen in Fig. 2, the winding of χ does not imply a discontinuity in the texture $\hat{\mathbf{n}}(\mathbf{r})$, unlike in an ordinary vortex, since the magnetization points toward the north pole near the origin. Yet any set of k points that are angularly spaced by $\Delta\alpha = 2\pi/k$ for the same r all have the same magnetization $\hat{\mathbf{n}}$ at them, showing that this is a k-to-1 texture, which constitutes a k defect at the origin. Although this field is continuous, it is not possible to smooth the defect by altering the orientation of the vectors while keeping a single-signed Jacobian; the defect will merely be relocated to another position.

The presence of these defects in the system is dictated by the Riemann-Hurwitz formula, a topological theorem that establishes a relationship between the branching points in a mapping and the topological properties of the spaces it connects. We will assume that, away from defects, the mapping is differentiable and has a positive Jacobian. Let P and S be two closed Riemann surfaces, and let $\hat{\mathbf{n}} : P \to S$ represent the mapping between the spaces. Then each point of S, except for images of defects, must be mapped to the same number of times, say, Q [56–58]. Suppose that $\hat{\mathbf{n}}$ has defects at N different points of P, where these defects possess the topological numbers $k_1, \ldots, k_N$. Then the Riemann-Hurwitz formula states that

$$2p - 2 = (2s - 2)Q + \sum_{i=1}^{N} (k_i - 1), \quad (9)$$

where $p = \text{genus}(P)$ and $s = \text{genus}(S)$ [59–62].

In our case, $\hat{\mathbf{n}}(\mathbf{r})$ is a mapping from the unit cell P on the plane to the sphere of spin states S. The genus of P is $p = 1$ as the unit cell is topologically equivalent to a torus, and the genus of S is $s = 0$. Therefore, the Riemann-Hurwitz formula (9) yields

$$2Q = \sum_{i=1}^{N} (k_i - 1). \quad (10)$$

This formula leads to a significant conclusion: stable defects with $k \geqslant 2$ *must* exist in the system. The formula further emphasizes that a $k = 1$ texture does not describe a defect; $k = 1$ points do not contribute to the Riemann-Hurwitz formula. It is important to note that these defects not only appear in excited states, but are intrinsic features manifesting even in the ground state of rotating systems. This parallels the presence of point defects in the ground state of an ordinary rotating superfluid.

The Riemann-Hurwitz formula provides the number of defects N in each unit cell. Specifically, if all the defects share the same k value, the number of defects in each unit cell is

$$N = \frac{2Q}{k - 1}. \quad (11)$$

Using Eq. (7), we find the density of defects in the system:

$$\frac{N}{A} = \frac{1}{\pi F(k - 1)} \frac{m\omega}{\hbar}. \quad (12)$$

Note that Q does not appear in this identity. For a specific condensate rotating at angular velocity ω, the density of the realized defects depends only on their k value.

The formula for the density of defects remains the same for finite F values, since the number of defects per unit cell is unchanged (the Riemann-Hurwitz formula applies even if the Jacobian of the mapping is not constant, as long as its sign is) and the integration result of the Mermin-Ho relation remains valid [41]. Notably, for $F = 1$ and $k = 2$, this formula coincides with the Feynman relation for ordinary vortex lattices [63]. We would like to again underscore the significance of the results derived from the remarkable Riemann-Hurwitz formula: it provides us with a prediction of distinct class of topological defects, separate from the conventional topological point defects characterized by the fundamental homotopy group.

As previously discussed, describing the spin texture for $F = \infty$ involves finding an equal-area mapping from the unit cell to the sphere. Although infinitely many such mappings exist, explicitly constructing one remains a challenging task. This paper focuses on explaining the topological structure of the mappings and how considering the topological defects aids in understanding it.

We assume Q should be as small as possible for the ground state, in order to achieve a simple topology. For a constant-sign Jacobian, every point in S has Q preimages in P. Thus, it is not possible to have $Q = 1$, as it would describe a 1-to-1 mapping, a homeomorphism, which contradicts the topological inequivalence between the torus and the sphere.

In order to find a $Q = 2$ mapping, we examine the arrangement of the point defects, since their positions and their images on the sphere determine qualitatively the rest of the mapping. Assuming all the defects of the mapping are of the simplest kind, namely, $k = 2$, the Riemann-Hurwitz formula (11) implies that each unit cell must contain $N = 4$ defects. The mapping can take various forms, each associated with

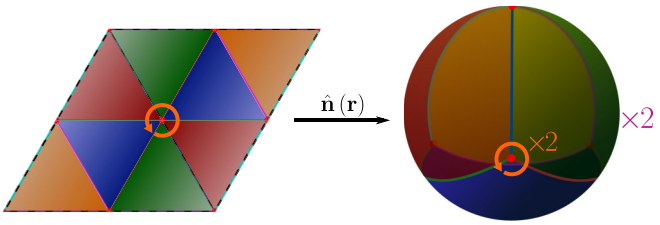

FIG. 3. The magnetization texture mapping $\hat{\mathbf{n}}(\mathbf{r})$ is obtained by dividing the plane into triangles and mapping them to spherical triangles indicated by matching colors (the orange triangle is in the back of the sphere). $k = 2$ defects (red points) are located at the vertices of the triangles, with $N = 4$ of them per unit cell. The images of the defects are arranged in the shape of a tetrahedron on the sphere. Each unit cell covers the sphere $Q = 2$ times, as the two triangles outlined in dashed black lines each close up to form one tetrahedron.

different energy dictated by the second term in Eq. (6) (the first term vanishes for area-preserving mappings). To identify the ground state mapping and find the defect positions, one must minimize this energy term. However, since ground states typically exhibit higher symmetry, and considering the rotational symmetry inherent in the problem, it is reasonable to focus on defect configurations with greater symmetry. A natural choice is to arrange the defects on the sphere in a tetrahedral configuration.

Now that the four defects are in place, we divide the sphere into four spherical triangles with the defect points at their corners (see Fig. 3). This configuration is then straightened out into a tetrahedron with flat faces in some equal-area manner. The four faces of the tetrahedron are then unfolded to form a triangle in the plane (dashed black lines in Fig. 3). Placing two such triangles side by side with reversed orientations forms a parallelogram unit cell, which can be repeated to tile the entire plane. This construction defines a mapping from the sphere to the plane, which can be inverted to obtain $\hat{\mathbf{n}}(\mathbf{r})$. The resulting map is double covering ($Q = 2$) because each parallelogram unit cell consists of the two triangles, with each triangle covering the sphere once under the mapping. On the plane, the defects are the points around which the corresponding faces of the tetrahedron are repeated twice, resulting in a 2-to-1 texture around them.

Numerical minimization of energy (6) using a steepest descent algorithm confirms that the actual ground state has the same topological structure as the mapping shown in Fig. 3, manifesting a triangular lattice with tetrahedrally arranged defects on the sphere. This structure remains the same for all spin values. These results are consistent with the prediction of a triangular lattice for pseudospin-1/2 and spin-1 systems in Refs. [3,4] and its experimental observation for pseudospin-1/2 [64]. However, the previous analyses have predominantly focused on separate spinor components, unlike our approach, which adopts a geometrical SO(3) symmetric viewpoint and reveals the presence and significance of the defects.

Thus far, our analysis has focused on understanding the defects through their influence on the magnetic structure. However, due to the Mermin-Ho relation, they also have a crucial effect on the condensate flow. To explore this, we relax the constraint $\mathbf{v} = \boldsymbol{\omega} \times \mathbf{r}$, allowing us to explore the ground state of a system with large yet finite F, utilizing the Euler-Lagrange equations derived from energy (6).

It can be shown that for an area-preserving mapping the second spatial derivatives of $\hat{\mathbf{n}}$ diverge at the defects, causing the torque $\delta E/\delta\phi$ acting on $\hat{\mathbf{n}}$ to diverge. Consequently, such a mapping is valid only for infinite F; for any finite F, a different solution is required near the defects. To address this, we study the cores of the defects, defined as the regions where the area-preserving approximation breaks down significantly, and characterized by a notable deviation of the vorticity from the rigid rotation value $2\boldsymbol{\omega}$, as can be seen in Fig. 1. This definition differs from the definition of a typical defect core, such as in scalar superfluid vortices, which is based on a significant reduction in density. In this sense, the defects we describe are coreless.

In the large-F limit, the core size is found to be independent of F. Since areas are scaled by $1/F$ in the mapping to the unit sphere according to Eq. (7), the area corresponding to the image of the core on the sphere is proportional to F^{-1}, hence its angular size scales as $\phi \sim F^{-\frac{1}{2}}$ (when $\hat{\mathbf{n}}$ at the defect is rotated to the north pole). For large F, this region is small and thus approximately flat, allowing us to simplify the Euler-Lagrange equations in this region by neglecting the curvature of the sphere. Assuming a rotationally invariant structure in the vicinity of the defect, we may take $\chi = k\alpha$ in order to describe a k defect. The approximated Euler-Lagrange equation for ϕ is then:

$$x\frac{\partial}{\partial x}\left(x\frac{\partial u}{\partial x}\right) = k^2[(1-x^2)u + u^3], \tag{13}$$

where $u = \sqrt{F}\phi$, and $\mathbf{x} = \sqrt{m\omega/\hbar k}\mathbf{r}$ is a dimensionless form of the coordinates. Since this equation is independent of the parameters, the typical scales for u and x are of order 1, justifying the scales mentioned earlier. In the original variables, the core area on the plane is of order $m\omega/\hbar$; therefore, for large F, the unit cell size [Eq. (7)] is much larger than the core size. Hence, the cores are far apart, validating the analysis of each core separately. While $u \propto x$ near the defect

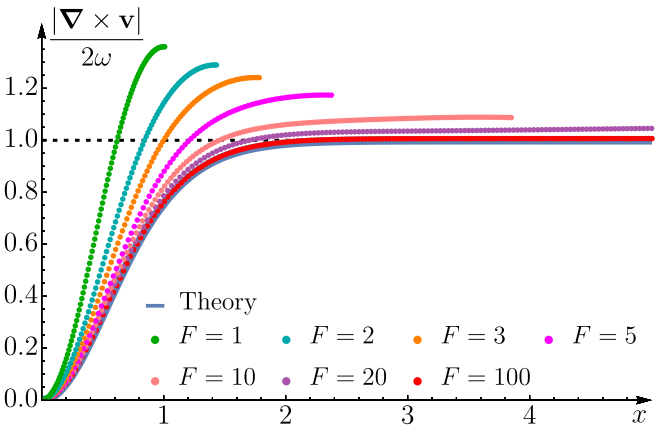

FIG. 4. Blue curve: vorticity around a $k = 2$ defect, calculated from Eq. (14) using the numerical solution of (13). Points: numerical gradient descent simulation results for the angle-averaged vorticity around a $k = 2$ defect for various values of F.

for the area-preserving case, the solution of Eq. (13) yields $u \propto x^k$. This corrects the aforementioned singularities in the second derivatives of $\hat{\mathbf{n}}$, resulting in an infinitely differentiable magnetization texture.

After rescaling, the Mermin-Ho relation around the defect becomes

$$\nabla \times \mathbf{v} = 2\boldsymbol{\omega}\frac{u}{x}\frac{\partial u}{\partial x}. \tag{14}$$

Numerical solution of Eq. (13) for $u(x)$ yields the vorticity inside the core, shown in Fig. 4. The vorticity grows from 0 to 2ω on the scale of $x \approx 1$, consistent with the expected core size. Comparison with vorticity of the defects in the numerical results shows convergence towards the predicted curve as F increases. Besides leading to a finite core size, a finite F has interesting effects on the vorticity outside the core: its mean exceeds 2ω (see Fig. 4), and it is smaller along valleys connecting the defects (see Fig. 1). These corrections will be addressed in [41].

The distinction between the velocity field defects in our system and conventional superfluid vortices is evident. Here vorticity increases gradually from zero at the defect point to $2\boldsymbol{\omega}$ with distance, whereas in regular superfluid vortices all the vorticity is concentrated within the defect itself. This analysis, supported by independent numerical results, shows that the positions of these "unvortices" align precisely with the locations of the magnetic texture defects. This alignment establishes a direct connection between the defects of $\mathbf{v}(\mathbf{r})$ and $\hat{\mathbf{n}}(\mathbf{r})$, despite their fundamentally different nature.

We would like to thank Hillel Aharoni for suggesting the term "unvortex" and Sandro Stringari for promoting initial interest in the problem of rigidly rotating superfluids. R.B. acknowledges support from the European Union's Seventh Framework Programme under Grant No. PCIG-GA2013-631002. The work at the Technion was supported by Grant ISF 1939/18. R.B. and A.M.T. are grateful for the hospitality of the Aspen Center for Physics under Grant No. PHYS-1066293.

[1] N. D. Mermin and T.-L. Ho, Circulation and angular momentum in the a phase of superfluid helium-3, Phys. Rev. Lett. **36**, 594 (1976).
[2] Y. Kawaguchi and U. Masahito, Spinor Bose–Einstein condensates, Phys. Rep. **520**, 253 (2012).
[3] E. J. Mueller and H. Tin-Lun, Two-component Bose-Einstein condensates with a large number of vortices, Phys. Rev. Lett. **88**, 180403 (2002).
[4] J. W. Reijnders, F. J. M. van Lankvelt, and K. Schoutens, Rotating spin-1 bosons in the lowest Landau level, Phys. Rev. A **69**, 023612 (2004).
[5] S. Yi and H. Pu, Spontaneous spin textures in dipolar spinor condensates, Phys. Rev. Lett. **97**, 020401 (2006).
[6] Y. Kawaguchi, H. Saito, and M. Ueda, Einstein–de Haas effect in dipolar Bose-Einstein condensates, Phys. Rev. Lett. **96**, 080405 (2006).
[7] W. Zhang, Ö. E. Müstecaplıoğlu, and L. You, Solitons in a trapped spin-1 atomic condensate, Phys. Rev. A **75**, 043601 (2007).
[8] T. P. Simula, J. A. M. Huhtamäki, M. Takahashi, T. Mizushima, and K. Machida, Rotating dipolar spin-1 Bose–Einstein condensates, J. Phys. Soc. Jpn. **80**, 013001 (2011).
[9] R. W. Cherng and E. Demler, Neutral skyrmion configurations in the low-energy effective theory of spinor-condensate ferromagnets, Phys. Rev. A **83**, 053614 (2011).
[10] S. W. Song, L. Wen, C. F. Liu, S. C. Gou, and W. M. Liu, Ground states, solitons and spin textures in spin-1 Bose-Einstein condensates, Front. Phys. **8**, 302 (2013).
[11] C.-C. Huang and S.-K. Yip, Dynamics and complex structure of two-dimensional skyrmions in antiferromagnetic spin-1 Bose-Einstein condensates, Phys. Rev. A **88**, 013628 (2013).
[12] T. Kaneda, Dynamics of a vortex dipole across a magnetic phase boundary in a spinor Bose-Einstein condensate, Phys. Rev. A **90**, 053632 (2014).
[13] S. W. Seo, S. Kang, W. J. Kwon, and Y. I. Shin, Half-quantum vortices in an antiferromagnetic spinor Bose-Einstein condensate, Phys. Rev. Lett. **115**, 015301 (2015).
[14] T. Mawson, G. Ruben, and T. Simula, Route to non-Abelian quantum turbulence in spinor Bose-Einstein condensates, Phys. Rev. A **91**, 063630 (2015).
[15] M. O. Borgh, M. Nitta, and J. Ruostekoski, Stable core symmetries and confined textures for a vortex line in a spinor Bose-Einstein condensate, Phys. Rev. Lett. **116**, 085301 (2016).
[16] Y. Li, Z. Luo, Y. Liu, Z. Chen, C. Huang, S. Fu, H. Tan, and B. A. Malomed, Two-dimensional solitons and quantum droplets supported by competing self-and cross-interactions in spin-orbit-coupled condensates, New J. Phys. **19**, 113043 (2017).
[17] E. B. Sonin, Spin and mass superfluidity in a ferromagnetic spin-1 Bose-Einstein condensate, Phys. Rev. B **97**, 224517 (2018).
[18] R. Zamora-Zamora and V. Romero-Rochín, Skyrmions with arbitrary topological charges in spinor Bose–Einstein condensates, J. Phys. B **51**, 045301 (2018).
[19] H. B. Luo, L. Li, and W. M. Liu, Three-dimensional skyrmions with arbitrary topological number in a ferromagnetic spin-1 Bose-Einstein condensate, Sci. Rep. **9**, 18804 (2019).
[20] T. Mithun, R. Carretero-González, E. G. Charalampidis, D. S. Hall, and P. G. Kevrekidis, Existence, stability, and dynamics of monopole and Alice ring solutions in antiferromagnetic spinor condensates, Phys. Rev. A **105**, 053303 (2022).
[21] J.-P. Martikainen, A. Collin, and K.-A. Suominen, Coreless vortex ground state of the rotating spinor condensate, Phys. Rev. A **66**, 053604 (2002).
[22] A. E. Leanhardt, Y. I. Shin, D. Kielpinski, D. E. Pritchard, and W. Ketterle, Coreless vortex formation in a spinor Bose-Einstein condensate, Phys. Rev. Lett. **90**, 140403 (2003).
[23] T. Mizushima, N. Kobayashi, and K. Machida, Coreless and singular vortex lattices in rotating spinor Bose-Einstein condensates, Phys. Rev. A **70**, 043613 (2004).
[24] K. Kasamatsu, M. Tsubota, and M. Ueda, Vortices in multicomponent Bose–Einstein condensates, Int. J. Mod. Phys. B **19**, 1835 (2005).

[25] J. Lovegrove, M. O. Borgh, and J. Ruostekoski, Energetically stable singular vortex cores in an atomic spin-1 Bose-Einstein condensate, Phys. Rev. A **86**, 013613 (2012).
[26] X. Q. Xu and J. H. Han, Spin-orbit coupled Bose-Einstein condensate under rotation, Phys. Rev. Lett. **107**, 200401 (2011).
[27] M. D. Barrett, J. A. Sauer, and M. S. Chapman, All-optical formation of an atomic Bose-Einstein condensate, Phys. Rev. Lett. **87**, 010404 (2001).
[28] M.-S. Chang, C. D. Hamley, M. D. Barrett, J. A. Sauer, K. M. Fortier, W. Zhang, L. You, and M. S. Chapman, Observation of spinor dynamics in optically trapped ^{87}Rb Bose-Einstein condensates, Phys. Rev. Lett. **92**, 140403 (2004).
[29] D. M. Stamper-Kurn, M. R. Andrews, A. P. Chikkatur, S. Inouye, H. J. Miesner, J. Stenger, and W. Ketterle, Optical confinement of a Bose-Einstein condensate, Phys. Rev. Lett. **80**, 2027 (1998).
[30] H. J. Miesner, D. M. Stamper-Kurn, J. Stenger, S. Inouye, A. P. Chikkatur, and W. Ketterle, Observation of metastable states in spinor Bose-Einstein condensates, Phys. Rev. Lett. **82**, 2228 (1999).
[31] A. T. Black, E. Gomez, L. D. Turner, S. Jung, and P. D. Lett, Spinor dynamics in an antiferromagnetic spin-1 condensate, Phys. Rev. Lett. **99**, 070403 (2007).
[32] S. Huh, K. Kim, K. Kwon, and J. Y. Choi, Observation of a strongly ferromagnetic spinor Bose-Einstein condensate, Phys. Rev. Res. **2**, 033471 (2020).
[33] T. Kuwamoto, K. Araki, T. Eno, and T. Hirano, Magnetic field dependence of the dynamics of ^{87}Rb spin-2 Bose-Einstein condensates, Phys. Rev. A **69**, 063604 (2004).
[34] H. Schmaljohann, M. Erhard, J. Kronjäger, M. Kottke, S. van Staa, L. Cacciapuoti, J. J. Arlt, K. Bongs, and K. Sengstock, Dynamics of $F = 2$ spinor Bose-Einstein condensates, Phys. Rev. Lett. **92**, 040402 (2004).
[35] A. Görlitz, T. L. Gustavson, A. E. Leanhardt, R. Löw, A. P. Chikkatur, S. Gupta, S. Inouye, D. E. Pritchard, and W. Ketterle, Sodium Bose-Einstein condensates in the $F = 2$ state in a large-volume optical trap Phys. Rev. Lett. **90**, 090401 (2003).
[36] Q. Beaufils, R. Chicireanu, T. Zanon, B. Laburthe-Tolra, E. Maréchal, L. Vernac, J.-C. Keller, and O. Gorceix, All-optical production of chromium Bose-Einstein condensates, Phys. Rev. A **77**, 061601 (2008).
[37] B. Pasquiou, E. Maréchal, G. Bismut, P. Pedri, L. Vernac, O. Gorceix, and B. Laburthe-Tolra, Spontaneous demagnetization of a dipolar spinor Bose gas in an ultralow magnetic field, Phys. Rev. Lett. **106**, 255303 (2011).
[38] K. Aikawa, A. Frisch, M. Mark, S. Baier, A. Rietzler, R. Grimm, and F. Ferlaino, Bose-Einstein condensation of erbium, Phys. Rev. Lett. **108**, 210401 (2012).
[39] Y. Miyazawa, R. Inoue, H. Matsui, G. Nomura, and M. Kozuma, Bose-Einstein condensation of europium, Phys. Rev. Lett. **129**, 223401 (2022).
[40] M. Lu, N. Q. Burdick, S. H. Youn, and B. L. Lev, Strongly dipolar Bose-Einstein condensate of dysprosium, Phys. Rev. Lett. **107**, 190401 (2011).
[41] R. Rabaglia, R. L. Barnett, and A. M. Turner (unpublished).
[42] D. Kleckner and W. T. Irvine, Creation and dynamics of knotted vortices, Nat. Phys. **9**, 253 (2013).
[43] D. Proment, M. Onorato, and C. F. Barenghi, Vortex knots in a Bose-Einstein condensate, Phys. Rev. E **85**, 036306 (2012).
[44] D. Kleckner, L. H. Kauffman, and W. T. Irvine, How superfluid vortex knots untie, Nat. Phys **12**, 650 (2016).
[45] C. Timm, S. M. Girvin, and H. A. Fertig, Skyrmion lattice melting in the quantum Hall system, Phys. Rev. B **58**, 10634 (1998).
[46] D. C. Wright and N. D. Mermin, Crystalline liquids: The blue phases, Rev. Mod. Phys. **61**, 385 (1989).
[47] S. M. Shamid, D. W. Allender, and J. V. Selinger, Predicting a polar analog of chiral blue phases in liquid crystals, Phys. Rev. Lett. **113**, 237801 (2014).
[48] A. Lamacraft, Low-energy dynamics of spinor condensates, Phys. Rev. B **81**, 184526 (2010).
[49] M. O. Borgh and J. Ruostekoski, Topological interface physics of defects and textures in spinor Bose-Einstein condensates, Phys. Rev. A **87**, 033617 (2013).
[50] A. Lamacraft, Long-wavelength spin dynamics of ferromagnetic condensates, Phys. Rev. A **77**, 063622 (2008).
[51] A. Lamacraft, Persistent currents in ferromagnetic condensates, Phys. Rev. B **95**, 224512 (2017).
[52] The contributions of centrifugal forces and trap potential may disrupt the assumption of constant density profile. However, except near the edges of the condensate, these effects can be neglected due to strong interatomic interactions, rendering them absent from the energy functional.
[53] S. Stringari, Diffused vorticity and moment of inertia of a spin-orbit coupled Bose-Einstein condensate, Phys. Rev. Lett. **118**, 145302 (2017).
[54] R. Rajaraman, *Solitons and Instantons. An Introduction to Solitons and Instantons in Quantum Field Theory* (Elsevier Science Publishers, Amsterdam, 1982).
[55] J. H. Han, *Skyrmions in Condensed Matter*, Springer Tracts in Modern Physics, Vol. 278 (Springer, Berlin, 2017).
[56] M. Monastyrsky, *Topology of Gauge fields and Condensed Matter* (Springer Science and Business Media, New York, 2013), pp. 125–134 and 223, Chap. 2.5.
[57] J. W. Milnor and D. W. Weaver, *Topology from the Differentiable Viewpoint* (Princeton University Press, Princeton, 1997), pp. 26–31, Chap. 5.
[58] G. von Gersdorff, S. Panahiyan, and W. Chen, Unification of topological invariants in Dirac models, Phys. Rev. B **103**, 245146 (2021).
[59] B. Riemann, *Gesammelte Mathematische Werke und Wissenschaftlicher Nachlass* (B. G. Teubner, 1876).
[60] A. Hurwitz, *Ueber Riemann'sche Flächen mit Gegebenen Verzweigungspunkte*, Mathematische Werke 1 (Birkhäuser, 1932), pp. 321–383.
[61] A. F. Beardon, *Iteration of Rational Functions: Complex Analytic Dynamical Systems*, Graduate Texts in Mathematics, Vol. 132 (Springer Science and Business Media, New York, 2000).
[62] S. Donaldson, *Riemann Surfaces*, Oxford Graduate Texts in Mathematics, Vol. 22 (Oxford University Press, Oxford, 2011).
[63] R. P. Feynman, *Application of Quantum Mechanics to Liquid Helium*, in *Progress in Low Temperature Physics* (Elsevier, 1955), Vol. 1, pp. 17–53.
[64] V. Schweikhard, I. Coddington, P. Engels, S. Tung, and A. E. Cornell, Vortex-lattice dynamics in rotating spinor Bose-Einstein condensates, Phys. Rev. Lett. **93**, 210403 (2004).